




Structural diversity, large interlayer spacing and switchable electronic properties of graphitic systems

Qiaoyi Han¹, Kun Luo^{1,2,*} , Lei Sun¹, Quan Huang³, Bing Liu¹, Qi Gao¹, Zihe Li¹, Pan Ying^{1,2}, Zhisheng Zhao¹, Bo Xu¹, and Julong He^{1,*}

¹Center for High Pressure Science (CHiPS), State Key Laboratory of Metastable Materials Science and Technology, Yanshan University, Qinhuangdao 066004, People's Republic of China

²Key Laboratory for Microstructural Material Physics of Hebei Province, School of Science, Yanshan University, Qinhuangdao 066004, People's Republic of China

³School of Materials and Chemical Engineering, Zhongyuan University of Technology, Zhengzhou 450007, People's Republic of China

Received: 24 October 2020

Accepted: 3 December 2020

Published online:

3 January 2021

© The Author(s), under exclusive licence to Springer Science+Business Media, LLC part of Springer Nature 2021

ABSTRACT

Recent experiments reported a substantial toughening of nanotwinned diamond (nt-diamond) composite with coherently interfaced diamond polytypes (different stacking sequences). This discovery emphasizes the diversity of graphite-like structures in carbon onion precursors for synthesizing nt-diamond composite. We designed five new graphitic polytypes to investigate structural diversity in graphitic systems. Under ambient pressure, the energies of all the proposed polytypes are between those of graphite (AB structure) and a previously predicted AA structure. Dynamic and elastic stability results showed that four structures (AB'C', AB'D', AAB and ABCB) can be stable under ambient pressure. These four structures all have a large interlayer distance comparable to those in carbon onion and turbostratic graphite. Chiral graphitic structures (AB'D' and AB'C') with reversible electrical properties under slight stress might be responsible for the controversy about the bandgap of graphitic samples. Therefore, these four structures are most likely to be a part of the structures existing in carbon onion and turbostratic graphite or are structural defects in graphitic samples.

Handling Editor: David Cann.

Address correspondence to E-mail: hiluokun@gmail.com; hjl@ysu.edu.cn

<https://doi.org/10.1007/s10853-020-05657-5>

Introduction

Graphitic systems are a large group of materials that consist of Van der Waals-coupled graphene layers [1, 2]. These materials have a wide variety of industrial applications as lubricant and refractory materials, neutron moderators in nuclear fission reactors [3–5] and other applications in energy conversion and storage devices [6–10]. In graphitic systems, every layer of graphene easily shift and twist in the horizontal plane because of the weak Van der Waals interlayer bonding. Thus, graphitic systems, including graphite [1], multilayer graphenes [11], turbostratic graphite [2, 12] and carbon onion [13], possess rich allotropic structures with different stacking sequences. In addition to the (unavoidable) disordered (turbostratic) fraction, there are two types of stacking, namely AB stacking (2H-graphite) with hexagonal symmetry and ABC stacking (3R-graphite) with rhombohedral symmetry in natural and synthetic graphitic flakes [1, 14–16]. Until now, many different stacking sequences of graphene have been researched, including AAA [11, 17–19], AAB [11, 20–22], ABA [22–25], ABC [22, 23, 25–28], twisted stacking sequences [18, 22, 29, 30] and turbostratic stacking sequences [31]. Carbon onion and turbostratic graphite with graphitic layers randomly oriented along the *c*-axis are composed of graphite domains in the usual (AB and ABC stacking) form and surrounded by different metastable graphitic structures [12, 13, 32, 33]. In short, graphitic systems are composed of high-symmetry graphitic structures with different degrees of stacking order.

Two high-symmetry graphitic structures (AA and AB') were proposed for the theoretical research of graphitic systems [12–14, 32–36] besides the usual (AB and ABC stacking) form of graphite [1, 14–16]. A variety of experimental phenomena have been explained by these graphitic structures: electrical properties (controversy about band gap) [4, 14, 33, 37], transformation path of graphite to diamond [34, 36], large interlayer spacing [35] and ultralow friction behavior [32] of turbostratic graphite. However, these researches [12–14, 32–36] may have been eclipsed by the high energy and instability of the two theoretical structures (AA and AB'). Furthermore, carbon onion precursors can transform in different pressures and temperatures into pure 3C nanotwinned diamond (nt-diamond) [38] and non-3C

polytype diamonds, such as 2H, 3R, 9R and 15R polytypes [39]. Thus, other graphitic structures with different stacking orders should be present in carbon onion precursor or appear during the synthesis of nt-diamond composite materials. In fact, it has been a consensus that different graphitic polytypes can transform to different sp^3 carbon allotropes or sp^2 – sp^3 hybrid intermediate carbon phase [40–43]. Particularly, recent studies [44, 45] have described two new families of diamond-graphene (diaphite) phases constructed from layered and bonded sp^3 and sp^2 nanostructural units. As the intermediate phase, they provide low-energy solutions to structural transformation between fully sp^2 and sp^3 bonded carbon allotropes [44, 45]. These unique nanostructures are complexity and could be engineered to improve fracture toughness among diamond materials [44, 45]. Therefore, systemic and full research on stable and low-energy graphitic structures with different stacking orders is crucial to understand whole graphitic systems and the transformation between sp^2 and sp^3 bonded carbon allotropes.

Here, five graphitic structures were theoretically constructed to investigate structural diversity in graphitic systems. All of the proposed graphitic structures were energetically more favorable than a previously predicted AA structure [11, 17–19]. The energy of ABCB was only 0.03 meV atom⁻¹ higher than that of 2H-graphite at ambient pressure. Four graphitic structures (AB'C', AB'D', AAB and ABCB) were stable at ambient pressure and had a large interlayer distance comparable to those of carbon onion and turbostratic graphite observed experimentally. The semimetal chiral graphitic structures (AB'D' and AB'C') will open the bandgap and become semiconductors under slight stress. This finding might be useful for understanding the inconsistent bandgaps of graphitic materials.

Computational methods

The graphitic structures of high-symmetry systems were constructed in the Materials visualizer module of materials studio software [46]. We built the new graphitic structures similar to a Lego game [47] by analyzing the existing interlayer relations (see Fig. 1a) of four previously investigated graphitic structures [12, 33, 35]. Five new combinations were retained after duplicates were removed. In this study,

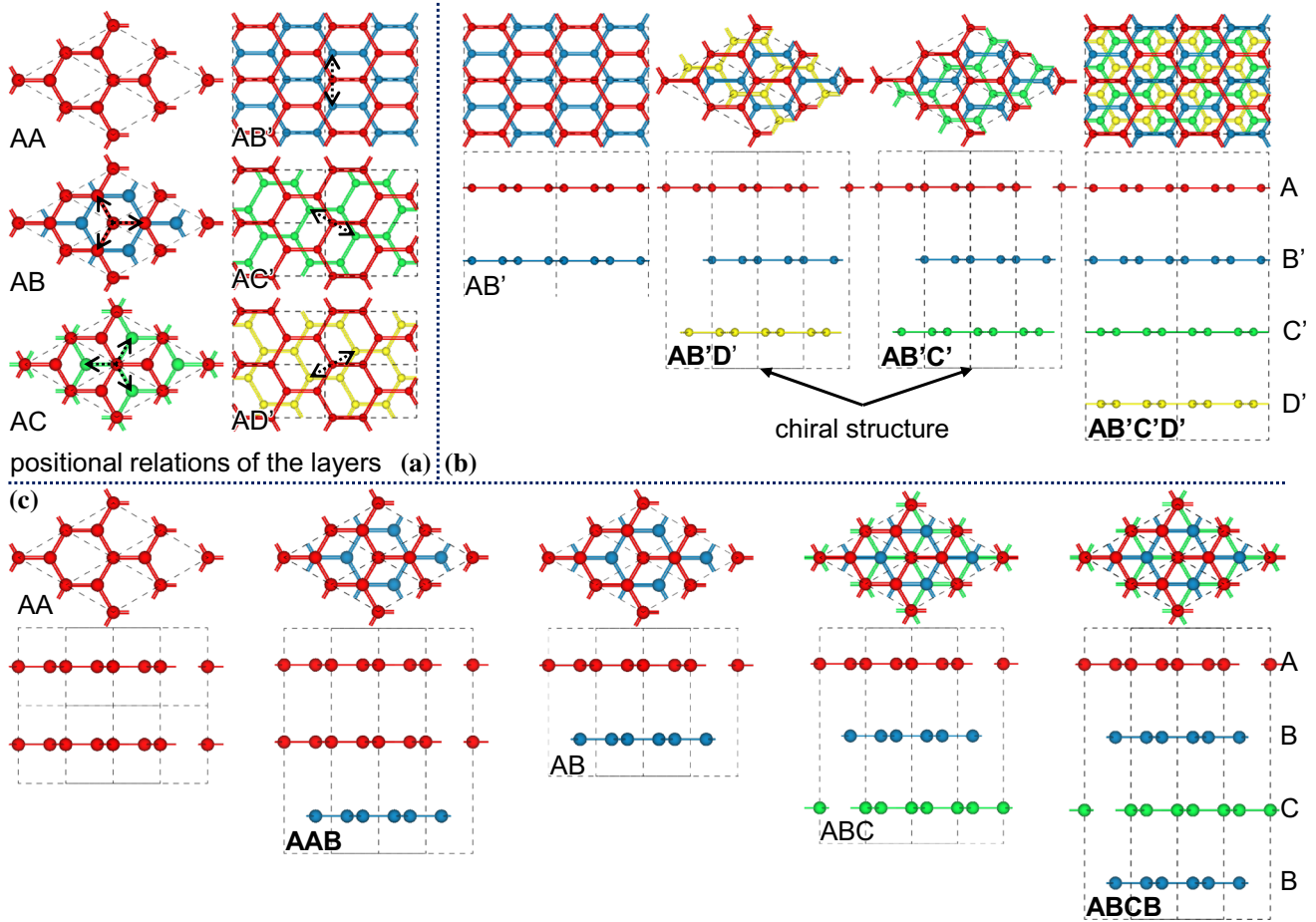


Figure 1 Top and side views of the high-symmetry graphitic structures investigated in this study. The structures are classified into two groups based on the precursor structure. **a** Interlayer relations of graphitic structures AA, AB, AC, AB', AC' and AD'.

b and **c** Graphitic structures with layer periodicity belong to groups AB' and AB. The structure proposed in this work is marked in bold.

all of the calculations were performed based on the density functional theory (DFT) as implemented in the CASTEP code [48]. Norm-conserving pseudopotentials were used [49]. A k -point sampling [50] of $0.03 \times 2\pi \text{ \AA}^{-1}$ and a plane-wave cutoff of 1000 eV were used. DFT with semi-empirical dispersion correction was adopted to describe the long-range Van der Waals interaction between carbon layers. The scheme developed by Ortmann, Bechstedt and Schmidt (OBS) [51] was used for DFT calculations with generalized gradient approximation in Perdew–Wang 91 (PW91) [52] functional form. The Broyden–Fletcher–Goldfarb–Shanno minimization scheme was used in geometry optimization [53]. Structural relaxation was stopped when the total energy change, maximum ionic displacement, stress and ionic Hellmann–Feynman force were less than 5.0×10^{-6} eV/

atom, $5.0 \times 10^{-4} \text{ \AA}$, 0.02 GPa and 0.01 eV \AA^{-1} , respectively. Standard DFT usually underestimates the bandgaps of semiconductors [54]. Thus, band structures were calculated using the DFT method with hybrid XC functional HSE06 to overcome the underestimation [55]. Considering the specific Dirac-cone-like bands in the graphitic systems, we specified a high-quality k -point set ($0.001 \times 2\pi \text{ \AA}^{-1}$) for the band structure calculation. Elastic constants were calculated in the linear elastic strain range. Phonon spectra were calculated via the linear response method [56, 57]. All symmetry k -points and symmetry k -lines in the Brillouin zone of primitive unit cells were determined by automatic flow (AFLOW) [58, 59]. The selected calculation parameters were tested to ensure that energy convergence was less than 1 meV atom^{-1} . Benchmark calculations were

conducted for 2H-graphite (AB structure) to validate our computational scheme and the results are summarized in Table 1. The calculated lattice parameters ($a = 2.461 \text{ \AA}$, $c = 6.697 \text{ \AA}$) were in good agreement with the experimental results ($a = 2.463 \text{ \AA}$, $c = 6.712 \text{ \AA}$ for the AB structure) [60]. The calculated bulk modulus of the AB structure was 38.6 GPa, which was in agreement with the experimental value of $36.4 \pm 11 \text{ GPa}$ [60].

Results

Structures

The high-symmetry graphitic structures are presented in Fig. 1. Based on six interlayer relations, namely AA, AB, AC, AB', AC' and AD' (Fig. 1a), which were mentioned in previous studies [12, 33–36], we obtained five new high-symmetry graphitic structures (Fig. 1b, c) in addition to the four previously investigated graphitic structures [32]. The novel proposed graphitic structures were designated as AB'D', AB'C', AB'C'D', AAB and ABCB, which were named according to the position of each layer in the unit cell. The structures generated by the translational gliding moves of the graphene layer in the zigzag and armchair directions were divided into groups AB' (Fig. 1b) and AB (Fig. 1c), respectively.

Remarkably, the AB'C' and AB'D' structures are mirror symmetry; thus, their crystals are chiral and

Table 1 Experimental and calculated lattice parameters (\AA), cell volume (C.V., \AA^3) and Bulk modulus (B , GPa) of 2H-graphite (AB structure) under ambient conditions. LDA (local density approximation), OBS (Ortmann–Bechstedt–Schmidt), PBE (Perdew–Burke–Ernzerhof), TS (Tkatchenko–Scheffler), Grimme, PW91 (Perdew–Wang 91)

Method	a	c	C.V	B
LDA [61, 62]	2.440	6.630	34.162	28.8
LDA + OBS [51]	2.432	6.159	31.546	64.6
PBE [63]	2.462	8.864	46.527	0.5
PBE + TS [64]	2.454	6.672	34.808	57.8
PBE + Grimme [65]	2.458	6.420	33.580	40.7
PW91 [52]	2.461	9.581	50.242	1.2
PW91 + OBS	2.461	6.697	35.113	38.6
Experimental [60]	2.463	6.712	35.262	36.4 ± 11

The method used in this article is shown in bold

cannot be superimposed on the mirror image. The different mirror images are called “enantiomers” or “optical isomers.” The AB'C'D' structure was constructed by adding one layer to each of the chiral structure to fill up the empty venues (top view in Fig. 1b). The AAB and ABCB structures are multi-layer graphenes [11, 20, 66–70], but no research has involved the corresponding bulk structures. The details of the high-symmetry graphitic structures are listed in Table S1 in the supplementary material. The lattice parameter a (2.461 \AA) of all of the structures is equal, whereas their average interlayer distances ($3.347\text{--}3.515 \text{ \AA}$) differ remarkably from each other. This result could be attributed to the strong intralayer covalent bonds and the weak interlayer Van der Waals bonds. The five proposed graphitic structures had longer interlayer distances than the most stable graphitic structure (AB structure). The longer distance might also be the origin for the larger interlayer spacing in turbostratic graphite [35] and carbon onion [13].

Stability and elastic properties

The thermodynamic stability of the five new graphitic structures was further examined by a direct enthalpy comparison with known theoretical

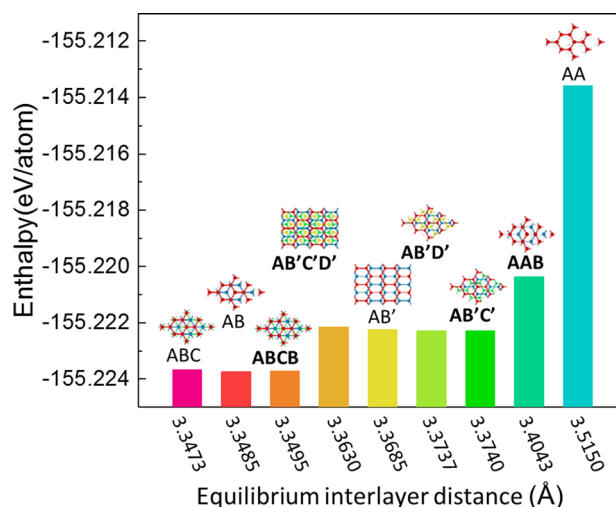


Figure 2 Enthalpy–interlayer distance relationship of the proposed new graphitic structures compared with other known experimental and theoretical graphitic structures at ambient pressure. All the proposed graphitic structures were energetically more favorable than the observed AA structure at ambient pressure. The structure proposed in this work is marked in bold.

graphitic structures in Fig. 2. Enthalpy is increased with the increase in interlayer distance. As shown in Fig. 2 and Table 2, the energies of the five proposed graphitic structures were lower than that of AA structure [11, 17–19] at ambient pressure and slightly higher than that of 2H-graphite (AB structure) by only 0.03–3.38 meV atom⁻¹. Interestingly, the chiral structures (AB'C' and AB'D') had lower energies and bigger interlayer distances than the AB' structure, which might exist in turbostratic graphite [32] for its large interlayer distance. Thus, the chiral structures likely exist in turbostratic graphite. In particular, the energy of ABCB was only 0.03 meV atom⁻¹ (the differences are beyond the accuracy of the calculations) higher than that of 2H-graphite at ambient pressure. Previous research showed that the energy of ABC structures is 0.07 meV atom⁻¹ higher than that of 2H-graphite at ambient pressure, which explains why the ABC structure (3R-graphite) is usually 5–15% intermixed with the perfect hexagonal one in natural graphitic flakes [1, 14–16]. Thus, ABCB likely exist in natural graphite. This characteristic can be understood because the proposed polytypes were constructed based on the existing interlayer relationships in the three graphitic structures [12, 33, 35]. Considering the large interlayer distance and relatively low energy of the proposed polytypes with respect to the previous AB' and AA structures, the five proposed polytypes might more likely exist in complex systems: natural graphite, turbostratic graphite and carbon onion [1, 12–16, 32, 33].

Their elastic constants were also calculated and are listed in Tables S2 and 3 to assess the elastic stability of our proposed graphitic structures. The elastic

stability criteria for hexagonal, trigonal and orthorhombic crystals were used in this survey [71–73]. All the five proposed structures satisfied the elastic stability criteria; thus, they are elastically stable at the ground state. The elastic stability of previous graphitic structures was also consistent with the results in Ref. [32]. The chiral structures of AB'C' and AB'D' were elastically stable in our study but not in Ref. [74]. Apparently, this difference can be attributed to not dealing with the requisite Van der Waals interaction of the graphitic systems in Ref. [74].

Note that C_{13} did not affect the stability; a positive (or negative) value means that the out-of-plane distance tends to expand (or contract) under in-plane compression. Elastic constants C_{11} and C_{12} describe in-plane deformations and possessed the highest values because of the strong sp^2 bonding interactions within the graphene planes. Elastic constant C_{33} describes out-of-plane compression or expansion and always had a positive value for different stacking orders (see Table 3). Elastic constants C_{44} and C_{55} correspond to the shear between graphene layers. The values of C_{44} and C_{55} were low and can be positive or negative depending on the stacking order because of the weak interaction between planes (see Table 3). These two elastic constants are very important as they can break the mechanical stability condition (i.e., C_{44} or $C_{55} < 0$). Compared with the negative elastic constant values (C_{44} or C_{55}) of AB' and AA structures, all the five proposed structures are more difficult to shear between graphene layers and are more stable in the c -axis.

The phonon spectra of the elastically stable structures were further calculated and are shown in

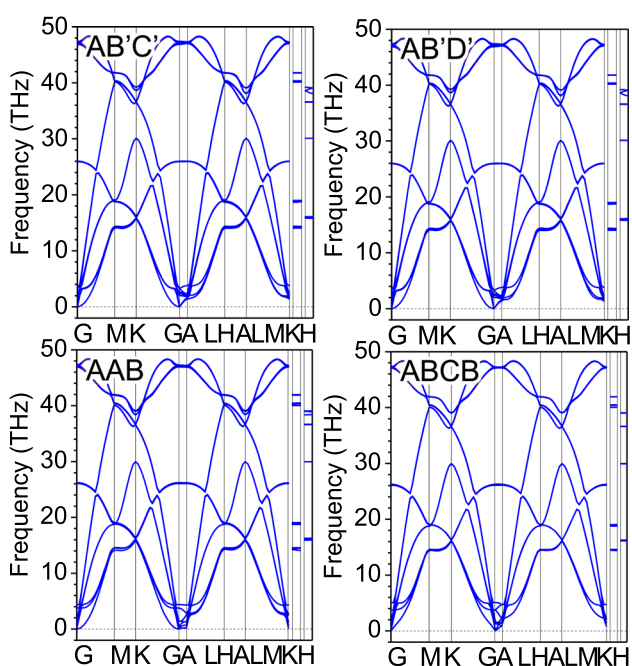
Table 2 Calculated structural information, mass density (g cm⁻³), equilibrium interlayer distance (d) and enthalpy differences (meV atom⁻¹) of various graphitic structures relative to those of 2H-graphite

Slip direction: positional relations of the layers	Structure	Space group	Density	d (Å)	Enthalpy difference
Zigzag direction: AB', AC', AD' Group AB' (Fig. 1b)	AB'	Fmmm (69)	2.258	3.369	1.50
	AB'D'	P6 ₄ 22 (181)	2.255	3.374	1.45
	AB'C'	P6 ₂ 22 (180)	2.255	3.374	1.45
	AB'C'D'	Fddd (70)	2.262	3.363	1.59
Armchair direction: AA, AB, AC Group AB (Fig. 1c)	AA	P6/mmm (191)	2.165	3.515	10.15
	AAB	P-6m2 (187)	2.235	3.404	3.38
	AB (2H-gra.)	P6 ₃ /mmc (194)	2.272	3.349	0.00
	ABC (3R-gra.)	R-3 m (166)	2.273	3.347	0.07
	ABCB	P6 ₃ /mmc (194)	2.271	3.350	0.03

at ambient pressure. The structure proposed in this work is marked in bold

Table 3 Elastic constants (GPa) for the different graphitic structures. The structure proposed in this work is marked in bold

Structure	C_{11}	C_{33}	C_{44}	C_{55}	C_{12}	C_{13}	Elastic stability	Dynamic stability
AB'	1042.0	42.7	− 2.5	7.7	179.4	− 5.1	Unstable	
AB'D'	1040.9	42.4	2.2	2.2	179.8	− 7.5	Stable	Stable
AB'C'	1040.8	42.5	2.2	2.2	179.8	− 7.5	Stable	Stable
AB'C'D'	1041.2	55.7	5.2	0.8	180.8	− 13.0	Stable	Unstable
AA	1001.7	43.2	− 4.8	− 4.8	172.1	− 9.1	Unstable	
AAB	1032.9	43.5	0.3	0.3	177.0	− 8.2	Stable	Stable
AB (2H-gra.)	1048.5	42.2	4.1	4.1	181.0	− 7.4	Stable	Stable
ABC (3R-gra.)	1048.9	43.0	4.1	4.1	181.2	− 7.3	Stable	Stable
ABCB	1048.0	41.9	4.1	4.1	181.4	− 7.5	Stable	Stable

**Figure 3** Phonon spectra of the proposed graphitic structures with dynamic stability at ambient pressure.

Figs. 3 and S1. The phonon spectra of the proposed structures AAB, ABCB and chiral structures (AB'C', AB'D') have no imaginary phonon frequency throughout the whole Brillouin zone; thus, they are dynamically stable. The results for AB'D' are completely different from Ref. [74], which indicates that reasonable dispersion correction is necessary for the research of layered materials. AB'C'D' was dynamically unstable because of the appearance of imaginary phonon frequency (Figures S1). According to our calculations, the chiral structures (AB'C' and AB'D'), AAB and ABCB are most likely a viable graphitic polytype as 3R-graphite (ABC) with low energy. By contrast, AB'C'D' might emerge as the

stacking faults in graphitic systems or as metastable phases that are stabilized by intercalated atoms in the same non-equilibrium environment as the AA and AB' structures [11, 17–19].

In all studies of theoretical graphitic structure to date, the four stable graphitic structure have very low energy and large interlayer distance. All of these advantages meant that the proposed chiral graphitic structures (AB'C' and AB'D'), AAB and ABCB could exist in graphitic systems just like 2H-graphite (AB) and 3R-graphite (ABC). Elastic constants C_{44} and C_{55} correspond to the shear between graphene layers. As shown in Table 3, the C_{44} and C_{55} values of the four structures were less than those of AB (2H-graphite) and ABC (3R-graphite). Thus, the large interlayer spacing [35] and ultralow friction behavior [32] of turbostratic graphite can be attributed to the existence of more stable graphitic structures (AB'C', AB'D', AAB and ABCB) than unstable AA and AB' structures.

Electronic properties

The electronic band structures of the four stable graphitic structures (AB'C', AB'D', AAB and ABCB) were calculated to clarify their influence on the electronic properties of graphitic systems. In different graphitic structures, strong intralayer bonding is described by sp^2 -hybridized $2s$, $2p_x$ and $2p_y$ atomic orbitals (σ states) and weak interlayer bonding is derived from the overlap between $2p_z$ orbitals (π states) perpendicular to the graphitic planes. The resulting band structure consists of bonding π and σ states and antibonding π^* and σ^* states that form the valence and conduction bands, respectively. The

weak interactions between graphitic planes modify the 2D situation (which leads to a zero-gap semiconductor [75]) and create a small overlap semimetal or small-gap semiconductor depending on the allotropic structure. Figure 4 shows the band structures of the four stable graphitic structures in the different special directions of the Brillouin zone determined by AFLOW [58, 59]. For comparison, the electronic band structures of the previously investigated graphitic structures are also shown in Figure S2. The effect of the stacking order on the main features of the band structures was very weak, besides the numbers of bands were different. The band structures of AB'C' and AB'D' look exactly alike because of their chirality. The chiral graphitic structures (AB'C' and AB'D') possess overlaps of 3 meV, whereas AAB and ABCB have overlaps of 31 and 4 meV, respectively. The electronic nature of a structure (semiconducting, semimetallic, or metallic) depends on the band structures in the region of the Fermi level. Figures S3 shows the detail of the band structures in the region

of the Fermi level and these graphitic structures are small-overlap semimetal.

Considering the influence of possible stress on the sample, we also investigated the electronic nature of these four stable graphitic structures under ± 1 GPa. Bandgap (overlap) variations with pressure are shown in Fig. 5. The four structures (AAB, ABCB, AB and ABC) had no substantial changes in electronic nature; the bandgap (overlap) only changed in value. However, the electronic nature of the chiral graphitic structures (AB'C' and AB'D') transformed from semimetal to semiconductor under slight positive or negative stress. This characteristic might be responsible for the controversy about the bandgap of graphitic materials [4, 14, 33, 37].

Conclusions

Five graphitic structures were theoretically designed to investigate the structural diversity of graphitic systems, particularly in the complex systems turbostratic graphite and carbon onion. These structures were energetically more favorable than the previously predicted AA structure at ambient pressure. The energy of ABCB was only 0.03 meV atom⁻¹ higher than that of 2H-graphite (AB structure). Four among the proposed structures (AB'D', AB'C', AAB and ABCB) had dynamic and mechanical stability, which indicate that these structures might be recoverable once formed. Their large *d* values are

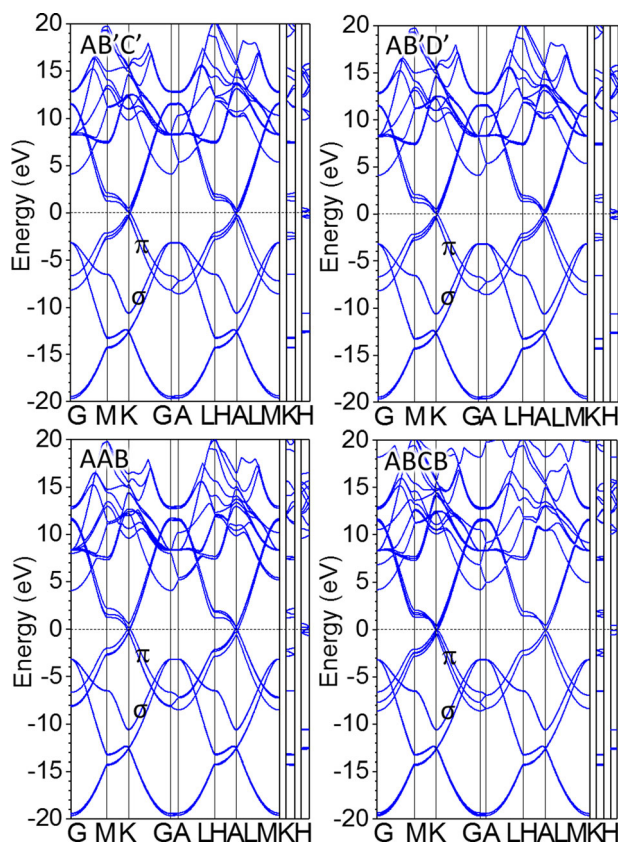


Figure 4 Band structures of the four stable graphitic structures calculated with the HSE06 functional at ambient pressure.

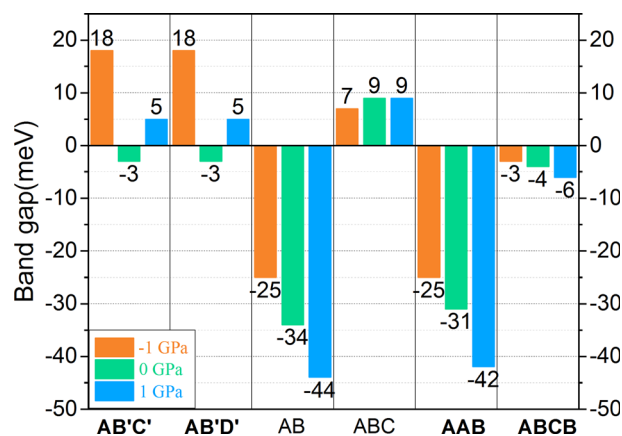


Figure 5 Variation in the band gap (overlap) versus pressure of six stable graphitic structures. The positive value of the band gap represents the band gap of the semiconductor and the negative value represents the degree of the overlap of the semimetal. The structure proposed in this work is marked in bold.

consistent with the characteristics of turbostratic graphite [35] and might be the origin for the larger interlayer spacing in turbostratic graphite and carbon onion. Moreover, the chiral graphitic structures (AB'D' and AB'C') are small-overlap semimetal at ambient pressure and can directly transform from semimetal to semiconductor under slight positive or negative stress. This transformation might be responsible for the controversy about the bandgap of graphitic materials. Several new graphitic structures proposed by this work will enrich the research of graphitic systems, help understand the structural complexity of carbon onion and aid in the further study of more challenging problems, such as the transformation between sp^2 and sp^3 bonded carbon allotropes [38] [40–45] [69].

Acknowledgements

This work was supported by the national key research and development program of China (Grant No. 2018YFA0305900) and the national natural science foundation of China (Grants Nos. 91963203, 51722209, 51272227 and 51525205). Z. Zhao acknowledges NSF for Distinguished young scholars of Hebei Province of China (Grants No. E2018203349). K. Luo also acknowledges the project funded by China postdoctoral science foundation (2017M620097).

Compliance with ethical standards

Conflict of interest The authors declare that they have no conflict of interests.

Supplementary Information: The online version contains supplementary material available at <http://doi.org/10.1007/s10853-020-05657-5>.

References

- [1] Lipson H, Stokes AR (1942) The structure of graphite. *Proc R Soc A Math Phys Eng Sci* 181:101–105. <https://doi.org/10.1098/rspa.1942.0063>
- [2] Oya A, Marsh H (1982) Phenomena of catalytic graphitization. *J Mater Sci* 17:309–322. <https://doi.org/10.1007/BF00591464>
- [3] Klimenkov VI (1962) Behavior of graphite in nuclear reactor stacks. *Sov J At Energy* 10:439–450. <https://doi.org/10.1007/BF01674506>
- [4] García N, Esquinazi P, Barzola-Quiquia J, Dusari S (2012) Evidence for semiconducting behavior with a narrow band gap of Bernal graphite. *New J Phys.* <https://doi.org/10.1088/1367-2630/14/5/053015>
- [5] Evans TE, Moyer RA, Burrell KH et al (2006) Edge stability and transport control with resonant magnetic perturbations in collisionless tokamak plasmas. *Nat Phys* 2:419–423. <https://doi.org/10.1038/nphys312>
- [6] Trogadas P, Fuller TF, Strasser P (2014) Carbon as catalyst and support for electrochemical energy conversion. *Carbon* 75:5–42. <https://doi.org/10.1016/j.carbon.2014.04.005>
- [7] Raccichini R, Varzi A, Passerini S, Scrosati B (2015) The role of graphene for electrochemical energy storage. *Nat Mater* 14:271. <https://doi.org/10.1038/nmat4170>
- [8] Li Y, Zhou W, Wang H et al (2012) An oxygen reduction electrocatalyst based on carbon nanotube–graphene complexes. *Nat Nanotechnol* 7:394. <https://doi.org/10.1038/nnano.2012.72>
- [9] Bonaccorso F, Colombo L, Yu G et al (2015) Graphene, related two-dimensional crystals and hybrid systems for energy conversion and storage. *Science* 347:41
- [10] Pumera M (2011) Graphene-based nanomaterials for energy storage. *Energy Environ Sci* 4:668–674. <https://doi.org/10.1039/c0ee00295j>
- [11] Que Y, Xiao W, Chen H et al (2015) Stacking-dependent electronic property of trilayer graphene epitaxially grown on Ru (0001). *Appl Phys Lett* 107:263101. <https://doi.org/10.1063/1.4938466>
- [12] Charlier JC, Michenaud JP, Lambin P (1992) Tight-binding density of electronic states of pregraphitic carbon. *Phys Rev B* 46:4540–4543. <https://doi.org/10.1103/PhysRevB.46.4540>
- [13] Choucair M, Stride JA (2012) The gram-scale synthesis of carbon onions. *Carbon* 50:1109–1115. <https://doi.org/10.1016/j.carbon.2011.10.023>
- [14] Charlier JC, Gonze X, Michenaud JP (1994) First-principles study of the stacking effect on the electronic properties of graphite (s). *Carbon* 32:289–299. [https://doi.org/10.1016/0008-6223\(94\)90192-9](https://doi.org/10.1016/0008-6223(94)90192-9)
- [15] Bacon G (1950) A note on the rhombohedral modification of graphite. *Acta Crystallogr* 3:320. <https://doi.org/10.1107/S0365110X50000872>
- [16] Gasparoux H (1967) Modification des propriétés magnétiques du graphite par création de séquences rhomboédriques. *Carbon* 5:441–451
- [17] Horiuchi S, Gotou T, Fujiwara M et al (2003) Carbon nanofilm with a new structure and property. *Jpn J Appl*

- Physics Part 2 Lett. 42:1073–1076. <https://doi.org/10.1143/JJAP.42.L1073>
- [18] Hwang J, Shields VB, Thomas CI et al (2010) Epitaxial growth of graphitic carbon on C-face SiC and sapphire by chemical vapor deposition (CVD). *J Cryst Growth* 312:3219–3224. <https://doi.org/10.1016/J.JCRYSGRO.2010.07.046>
- [19] Juang ZY, Wu CY, Lu AY et al (2010) Graphene synthesis by chemical vapor deposition and transfer by a roll-to-roll process. *Carbon* 48:3169–3174. <https://doi.org/10.1016/j.carbon.2010.05.001>
- [20] Rong ZY, Kuiper P (1993) Electronic effects in scanning-tunneling-microscopy-moire pattern on a graphite surface. *Phys Rev B* 48:17427–17431. <https://doi.org/10.1103/PhysRevB.48.17427>
- [21] Campanera JM, Savini G, Suarez-Martinez I, Heggie MI (2007) Density functional calculations on the intricacies of Moiré patterns on graphite. *Phys Rev B* 75:235449. <https://doi.org/10.1103/PhysRevB.75.235449>
- [22] Biedermann LB, Bolen ML, Capano MA et al (2009) Insights into few-layer epitaxial graphene growth on 4H-SiC(000 1) substrates from STM studies. *Phys Rev B* 79:125411. <https://doi.org/10.1103/PhysRevB.79.125411>
- [23] Lui CH, Malard LM, Kim S et al (2012) Observation of layer-breathing mode vibrations in few-layer graphene through combination Raman scattering. *Nano Lett* 12:5539–5544. <https://doi.org/10.1021/nl302450s>
- [24] Ellis CT, Stier AV, Kim M et al (2013) Magneto-optical fingerprints of distinct graphene multilayers using the giant infrared Kerr effect. *Sci Rep* 3:3143. <https://doi.org/10.1038/srep03143>
- [25] Lalmi B, Girard JC, Pallecchi E et al (2015) Flower-shaped domains and wrinkles in trilayer epitaxial graphene on silicon carbide. *Sci Rep* 4:4066. <https://doi.org/10.1038/srep04066>
- [26] Novoselov KS, Geim AK, Morozov SV et al (2004) Electric field effect in atomically thin carbon films. *Science* 306:666–669. <https://doi.org/10.1126/science.1102896>
- [27] Mak KF, Sfeir MY, Misewich JA, Heinz TF (2010) The evolution of electronic structure in few-layer graphene revealed by optical spectroscopy. *Proc Natl Acad Sci* 107:14999–15004. <https://doi.org/10.1073/pnas.1004595107>
- [28] Zhang L, Zhang Y, Camacho J et al (2011) The experimental observation of quantum Hall effect of $l=3$ chiral quasiparticles in trilayer graphene. *Nat Phys* 7:953–957. <https://doi.org/10.1038/nphys2104>
- [29] Cao Y, Fatemi V, Demir A et al (2018) Correlated insulator behaviour at half-filling in magic-angle graphene superlattices. *Nature* 556:80–84. <https://doi.org/10.1038/nature26154>
- [30] Cao Y, Fatemi V, Fang S et al (2018) Unconventional superconductivity in magic-angle graphene superlattices. *Nature* 556:43–50. <https://doi.org/10.1038/nature26160>
- [31] Lenski DR, Fuhrer MS (2011) Raman and optical characterization of multilayer turbostratic graphene grown via chemical vapor deposition. *J Appl Phys* 110:13720. <https://doi.org/10.1063/1.3605545>
- [32] Savini G, Dappe YJ, Öberg S et al (2011) Bending modes, elastic constants and mechanical stability of graphitic systems. *Carbon* 49:62–69. <https://doi.org/10.1016/j.carbon.2010.08.042>
- [33] Charlier JC, Michenaud JP, Gonze X (1992) First-principles study of the electronic properties of simple hexagonal graphite. *Phys Rev B* 46:4531–4539. <https://doi.org/10.1103/PhysRevB.46.4531>
- [34] Scandolo S, Bernasconi M, Chiarotti GL et al (1995) Pressure-induced transformation path of graphite to diamond. *Phys Rev Lett* 74:4015–4018. <https://doi.org/10.1103/PhysRevLett.74.4015>
- [35] Kolmogorov AN, Crespi VH (2005) Registry-dependent interlayer potential for graphitic systems. *Phys Rev B* 71:235415. <https://doi.org/10.1103/PhysRevB.71.235415>
- [36] Mailhot C, McMahan AK (1991) Atmospheric-pressure stability of energetic phases of carbon. *Phys Rev B* 44:11578–11591. <https://doi.org/10.1103/PhysRevB.44.11578>
- [37] Zoraghi M, Barzola-Quiquia J, Stiller M et al (2017) Influence of rhombohedral stacking order in the electrical resistance of bulk and mesoscopic graphite. *Phys Rev B* 95:045308. <https://doi.org/10.1103/PhysRevB.95.045308>
- [38] Huang Q, Yu D, Xu B et al (2014) Nanotwinned diamond with unprecedented hardness and stability. *Nature* 510:250–253. <https://doi.org/10.1038/nature13381>
- [39] Yue Y, Gao Y, Hu W et al (2020) Hierarchically structured diamond composite with exceptional toughness. *Nature* 582:370–374. <https://doi.org/10.1038/s41586-020-2361-2>
- [40] Boulfelfel SE, Oganov AR, Leoni S (2012) Understanding the nature of “superhard graphite.” *Sci Rep* 2:471. <https://doi.org/10.1038/srep00471>
- [41] Avery P, Wang X, Oses C et al (2019) Predicting superhard materials via a machine learning informed evolutionary structure search. *NPJ Comput Mater* 5:89. <https://doi.org/10.1038/s41524-019-0226-8>
- [42] Hoffmann R, Kabanov AA, Golov AA, Proserpio DM (2016) Homo citans and carbon allotropes: For an ethics of citation. *Angew Chemie Int Ed* 55:10962–10976. <https://doi.org/10.1002/anie.201600655>
- [43] Garvie LAJ, Nemeth P, Buseck PR (2014) Transformation of graphite to diamond via a topotactic mechanism. *Am Mineral* 99:531–538. <https://doi.org/10.2138/am.2014.4658>

- [44] Németh P, McColl K, Garvie LAJ et al (2020) Complex nanostructures in diamond. *Nat Mater* 19:1126–1131. <https://doi.org/10.1038/s41563-020-0759-8>
- [45] Németh P, McColl K, Smith RL et al (2020) Diamond-Graphene Composite Nanostructures. *Nano Lett* 20:3611–3619. <https://doi.org/10.1021/acs.nanolett.0c00556>
- [46] Materials Studio Program, version 7.0; Accelrys Inc.: San Diego, CA, 2012
- [47] Luo K, Yuan X, Zhao Z et al (2017) New hexagonal boron nitride polytypes with triple-layer periodicity. *J Appl Phys* 121:165102. <https://doi.org/10.1063/1.4981892>
- [48] Clark SJ, Segall MD, Pickard CJ et al (2005) First principles methods using CASTEP. *Zeitschrift für Krist-Cryst Mater* 220:567–570. <https://doi.org/10.1524/zkri.220.5.567.65075>
- [49] Hamann DR, Schlüter M, Chiang C (1979) Norm-conserving pseudopotentials. *Phys Rev Lett* 43:1494. <https://doi.org/10.1103/PhysRevLett.43.1494>
- [50] Monkhorst HJ, Pack JD (1976) Special points for Brillouin-zone integrations. *Phys Rev B* 13:5188. <https://doi.org/10.1103/PhysRevB.13.5188>
- [51] Ortmann F, Bechstedt F, Schmidt WG (2006) Semiempirical van der Waals correction to the density functional description of solids and molecular structures. *Phys Rev B* 73:205101. <https://doi.org/10.1103/PhysRevB.73.205101>
- [52] Perdew JP, Chevary JA, Vosko SH et al (1993) Erratum: Atoms, molecules, solids and surfaces: Applications of the generalized gradient approximation for exchange and correlation. *Phys Rev B* 48:4978. <https://doi.org/10.1103/PhysRevB.48.4978.2>
- [53] Pfrommer BG, Côté M, Louie SG, Cohen ML (1997) Relaxation of Crystals with the Quasi-Newton Method. *J Comput Phys* 131:233–240. <https://doi.org/10.1006/jcph.1996.5612>
- [54] Chan MKY, Ceder G (2010) Efficient band gap prediction for solids. *Phys Rev Lett* 105:196403. <https://doi.org/10.1103/PhysRevLett.105.196403>
- [55] Krukau AV, Vydrov OA, Izmaylov AF, Scuseria GE (2006) Influence of the exchange screening parameter on the performance of screened hybrid functionals. *J Chem Phys* 125:224106. <https://doi.org/10.1063/1.2404663>
- [56] Baroni S, Giannozzi P, Testa A (1987) Green's-function approach to linear response in solids. *Phys Rev Lett* 58:1861–1864. <https://doi.org/10.1103/PhysRevLett.58.1861>
- [57] Giannozzi P, de Gironcoli S, Pavone P, Baroni S (1991) Ab initio calculation of phonon dispersions in semiconductors. *Phys Rev B* 43:7231–7242. <https://doi.org/10.1103/PhysRevB.43.7231>
- [58] Setyawan W, Curtarolo S (2010) High-throughput electronic band structure calculations: Challenges and tools. *Comput Mater Sci* 49:299–312. <https://doi.org/10.1016/j.commatsci.2010.05.010>
- [59] Curtarolo S, Setyawan W, Hart GLW et al (2012) AFLOW: An automatic framework for high-throughput materials discovery. *Comput Mater Sci* 58:218–226. <https://doi.org/10.1016/j.commatsci.2012.02.005>
- [60] Bosak A, Krisch M, Mohr M et al (2007) Elasticity of single-crystalline graphite: Inelastic x-ray scattering study. *Phys Rev B* 75:153408. <https://doi.org/10.1103/PhysRevB.75.153408>
- [61] Ceperley DM, Alder BJ (1980) Ground state of the electron gas by a stochastic method. *Phys Rev Lett* 45:566–569. <https://doi.org/10.1103/PhysRevLett.45.566>
- [62] Perdew JP, Zunger A (1981) Self-interaction correction to density-functional approximations for many-electron systems. *Phys Rev B* 23:5048–5079. <https://doi.org/10.1103/physrevb.23.5048>
- [63] Perdew JP, Burke K, Ernzerhof M (1996) Generalized gradient approximation made simple. *Phys Rev Lett* 77:3865–3868. <https://doi.org/10.1103/PhysRevLett.77.3865>
- [64] Tkatchenko A, Scheffler M (2009) Accurate molecular Van Der Waals interactions from ground-state electron density and free-atom reference data. *Phys Rev Lett* 102:73004–73005. <https://doi.org/10.1103/PhysRevLett.102.073005>
- [65] Grimme S (2006) Semiempirical GGA-type density functional constructed with a long-range dispersion correction. *J Comput Chem* 27:1787–1799. <https://doi.org/10.1002/jcc.20495>
- [66] Torche A, Mauri F, Charlier JC, Calandra M (2017) First-principles determination of the Raman fingerprint of rhombohedral graphite. *Phys Rev Mater* 1:041001. <https://doi.org/10.1103/PhysRevMaterials.1.041001>
- [67] Lin CY, Wu JY, Ou YJ et al (2015) Magneto-electronic properties of multilayer graphenes. *Phys Chem Chem Phys* 17:26008–26035. <https://doi.org/10.1039/C5CP05013H>
- [68] Do TN, Lin CY, Lin YP et al (2015) Configuration-enriched magneto-electronic spectra of AAB-stacked trilayer graphene. *Carbon* 94:619–632. <https://doi.org/10.1016/j.carbon.2015.07.027>
- [69] Chiu CW, Chen RB (2016) Influence of electric fields on absorption spectra of AAB-stacked trilayer graphene. *Appl Phys Express* 9:065103. <https://doi.org/10.7567/APEX.9.065103>
- [70] Do TN, Chang CP, Shih PH, Lin MF (2017) Stacking-enriched magneto-transport properties of few-layer graphenes. *Phys Chem Chem Phys* 19:29525–29533. <https://doi.org/10.1039/c7cp05614a>

- [71] Born M (1940) On the stability of crystal lattices. I Math Proc Cambridge Philos Soc 36:160–172. <https://doi.org/10.1017/S0305004100017138>
- [72] Born M, Huang K (1954) Dynamical theory of crystal lattices. Am J Phys 23:474. <https://doi.org/10.1119/1.1934059>
- [73] Mouhat F, Coudert F-X (2014) Necessary and sufficient elastic stability conditions in various crystal systems. Phys Rev B 90:224104. <https://doi.org/10.1103/PhysRevB.90.224104>
- [74] Anees P, Valsakumar MC, Chandra S, Panigrahi BK (2014) Ab initio study on stacking sequences, free energy, dynamical stability and potential energy surfaces of graphite structures. Model Simul Mater Sci Eng 22:035016. <https://doi.org/10.1088/0965-0393/22/3/035016>
- [75] Wallace PR (1947) The Band Theory of Graphite. Phys Rev 71:622–634. <https://doi.org/10.1103/PhysRev.71.622>

Publisher's Note Springer Nature remains neutral with regard to jurisdictional claims in published maps and institutional affiliations.